Bacteroides uniformis regulates TH17 cell differentiation and alleviates chronic colitis by producing alpha-muricholic acid

Enping Zhang（✉ zhangenping@nwafu.edu.cn ）

Northwest A&F University

Yiting Yan

Northwest A&F University

Yu Lei

College of Animal Science and Technology, Northwest A&F University

Ying Qu

Northwest A&F University

Zhen Fan

Northwest A&F University

Ting Zhang

College of Animal Science and Technology, Northwest A&F University

Yangbin Xu

Northwest A&F University

Qian Du

Northwest A&F University

Daniel Brugger

Institute of Animal Nutrition and Dietetics, Vetsuisse-Faculty, University of Zurich

https://orcid.org/0000-0001-7267-0335

Yulin Chen

College of Animal Science and Technology, Northwest A&F University

Ke Zhang

Northwest A&F University

Article

Abstract

Inflammatory bowel disease (IBD) cause colitis-associated malignancy. Studies have shown that IBD development is associated with dysbiosis of the gut microbiota using the IBD model of animals and humans. *Bacteroides uniformis*, the most abundant core strain in mammals, regulates animal intestinal homoeostasis. However, the key metabolic compounds and mechanism by which *B. uniformis* treats colitis in mice are unknown. In this study, *B. uniformis* JCM5828-gavaged female C57BL/6 mice (n = 8) greatly alleviated the progression of DSS-induced colitis and restored the expression of mechanical and immune barrier proteins in the colon. Furthermore, increased abundance of *B. uniformis* in the colon promoted the abundance of the symbiotic bacteria *Bifidobacterium* and *Lactobacillus vaginalis* and inhibited the ecological niche of pathogenic *Escherichia coli*, thus regulating intestinal lipid metabolism function. Specifically, *B. uniformis* significantly increased the synthesis of primary and secondary bile acids (alpha-Muricholic acid (α-MCA), Isochenodeoxycholic acid (isoCDCA), hyodeoxycholic acid (HDCA), and isolithocholic acid (isoLCA)) in the colonic contents. *B. uniformis* also significantly regulated the expression of key regulator genes and proteins of the NF-κB and MAPK signaling pathways in colonic tissues and inhibited TH17 differentiation. *In vitro* cellular validation showed that single *B. uniformis* could not significantly inhibit TH17 differentiation in T lymphocytes. In contrast, key metabolic molecules α-MCA, HDCA and isoLCA could inhibit TH17 differentiation in the lamina propria and regulate the intestinal immune response. Cumulatively, the results indicate that *B. uniformis* JCM5828 supplementation may be an optional approach to the treat colitis and other diseases associated with intestinal barrier dysfunction.

Introduction

Inflammatory bowel disease (IBD) is a chronic non-specific inflammatory disease with unknown etiology. IBD mainly includes ulcerative colitis (UC) and Crohn's disease (CD) and is mostly common in the colon and rectum, with lesions confined to the mucosa and submucosa of the large intestine[1]. IBD has a protracted and recurrent course and infects 10 out of every 10,000 people globally[2]. The common therapies for IBD include probiotic preparations, glutamine analogues, and aminosalicylic acid preparations [3,4]. Adverse events during infancy can cause dysregulation of the host's intestinal microecology, resulting in the onset of IBD. IBD is most frequently manifested as dysregulation of the metabolism of tryptophan, bile acids, and short-chain fatty acids (SCFAs)[5]. IBD patients have reduced intestinal short-chain fatty acid levels and bile salt hydrolase activity. SCFAs can regulate mucosal immunity by promoting B-cell development, Treg differentiation and expansion, activation of inflammatory vesicles and IL-18 production[6]. Furthermore, bile acids can induce an immunomodulatory effect by activating receptors, such as farnesoid X receptor (FXR). Reduced bile salt hydrolase activity disrupts primary and secondary bile acid balance in IBD patients[7]. Interestingly, gut microbes regulate the abundance of these key metabolites. This suggests an effective means of preventing and treating the process of IBD using microbes that synthesize these molecules with high efficiency.

Bacteroides belong to the most prevalent and abundant members of the mammalian and rodent gut microbiota. *Bacteroides* have been used to provide colonization resistance to gut pathogens[8]. *Bacteroides* can compete with pathogens for host-derived amino acids (proline and hydroxyproline) and monosaccharides (ribose, fucose, arabinose, rhamnose, and fructose) and produce SCFAs, thus directly inhibiting pathogenesis[9]. Additionally, the evolutionary conserved enzyme class B-Hex, expressed by *Bacteroides* in the mouse intestine, can drive CD8aa-expressing intraepithelial lymphocytes (CD4IEL) differentiation. The B-Hex-specific lymphocytes can also suppress inflammation and protect the intestine in a mouse IBD model[10]. In addition, *B. thetaiotaomicron* produces bacterial extracellular vesicles (BEVs) on dendritic cells, macrophages and monocytes. The BEVs are released into the lumen of the intestine and can cross the mucus layer and enter the underlying immune cells, thereby suppressing intestinal inflammation[11]. *B. fragilis* can also prevent colon tumorigenesis, mainly by producing polysaccharide A. This process is mediated by TLR2 signaling to inhibit the expression of chemokine receptor CCR5 in the colon[12]. Furthermore, *B. uniformis* (Bu) is significantly and positively related to the reduction of early weaning-induced colonic inflammation in mammals[13]. However, it is unknown whether Bu reduces the incidence of chronic intestinal inflammation.

Genomic perspective studies have revealed that Bu can utilize β-glucans in the gut and may also share these glycans with human gut bacteria to potentially maintain gut microbial homeostasis[14]. Bu can prevent or reduce the incidence of the long-lasting IBD disease that affects humans. As a result, the use of Bu to promote the growth and durability of a better microbiota has recently attracted much attention. Bu can restore the ratio of lymphocytes and type 3 innate lymphoid cells in the intestinal epithelium, thereby reversing the metabolic and immune alterations that have an additive effect on diet-induced obesity[15]. However, no study has successfully assessed the probiotic processes of Bu, particularly the crucial metabolites of Bu activity and the cells targeted for action. Therefore, the action mechanisms of Bu in treating IBD should be determined for the application of a live, safe probiotic to enhance the health of IBD patients. This study aimed to evaluate the effects of Bu in the development of a mouse model of IBD. Oral administration of Bu increased beneficial commensal bacteria, including *Bacillus* and *Bifidobacterium*, and decreased proinflammatory bacteria, such as *Escherichia coli*, thereby creating a favorable and diverse microbial environment. Simultaneous metabolic production of more secondary bile acids inhibited the differentiation of colonic TH17, thus significantly decelerating IBD development. Therefore, this study may provide insights into the therapeutic use of Bu for IBD treatment and prevention.

Results

B. uniformis JCM5828 ameliorates DSS-induced chronic colitis

The DSS-induced C57BL/6 colitis mice were given Bu strain for 14 days to elucidate the remission effect of Bu on DSS-induced colitis in mice (Fig. 1A). Compared with the Con group, Bu treatment significantly alleviated the DSS-induced weight loss (Fig. 1B), and significantly decreased the DAI scores (Fig. 1C). In

addition, the Bu treatment substantially reduced colon inflammation compared to the Con group according to colon lengths and spleen weights (Fig. 1D-F). Bu treatment also reduced cumulative scores characterized by inflammatory infiltrates, goblet cell losses, crypt density, submucosal inflammation, and crypt abscesses compared with the Con group (Fig. 1G-H). Furthermore, Bu treatment significantly increased mucus layer thickness and the number of goblet cells in the colon (Fig. 1G-H), and the colonic mRNA and protein levels of *ZO-1*, Claudin-1, and Occludin as well (Fig. 1I and Fig. S1). Compared with the Con group, Bu treatment significantly decreased mRNA levels of *TNF-α*, *IL-6*, and *IL-1β* (Fig. 1J). These results suggested that *B. uniformis* can effectively restore the colonic mechanical and immune barriers and inhibit the secretion of proinflammatory cytokines, thus alleviating DSS-induced colitis.

B. uniformis JCM5828 reshapes gut microbiota and alleviates DSS-induced colitis

According to the Simpson, Chao and Shannon indexes, bacteria commensal richness and diversity significantly increased in the Bu group ($P < 0.05$, Fig. 2A). Principal coordinate analysis (PCoA) showed that the three groups had significantly different microbial community structures at the ASV level (ANOSIM, $r = 0.699$, $P = 0.001$, Fig. 2B). Also, Bu treatment significantly increased the abundance of Actinobacteriota in DSS mouse compared with the Con group at the phylum level ($P = 0.005$, Fig. S2A), and increased Bacteroides to Firmicutes (Bac/Fir) ratio from 0.17 to 0.61 ($P = 0.01$, Fig. 2C). Furthermore, Bu treatment significantly compensated for the lack of *Lactobacillus* ($P = 0.02$) and *Bacillus* ($P = 0.006$) abundance in the colon of DSS-induced colitis mice at the genus level, and significantly increased the abundance of *Bacteroides* ($P < 0.001$) and *Bifidobacterium* ($P = 0.02$, Fig. 2D and Table S1). Interestingly, Bu treatment significantly reduced the abundance of potentially pathogenic bacteria *Escherichia-Shigella* ($P = 0.001$) and *Romboutsia* ($P < 0.001$) in the colon of DSS-induced colitis mice (Fig. 2D, Table S1). Meanwhile, Bu treatment significantly increased the abundance of ASV346 (*Bacteroides*), ASV622 (*Bifidobacterium*), ASV85 (*Lactobacillus vaginalis*) at the ASV level, and decreased the abundance ASV178 (*Escherichia shigella*) and ASV92 (*Klebsiella*) (Fig. S2B). Phylogenetic tree showed that the gene sequences of three strains (ASV408, ASV346, ASV477) were closely related to *B. uniformis JCM5828* (Fig. 2E). The interaction network of the strains further showed that ASV346 (*Bacteroides*) cooperated with ASV408 (*Bacteroides*), ASV477 (*Bacteroides*), ASV627 (*Bifidobacterium*), ASV 1504 (*Romboutsia*) to inhibit the abundance of ASV462 (*Muribaculum*), and ASV399 (*Alistipes*) ($r = 0.6$, $P < 0.05$; Fig. 2F). The biomarkers with biological consistency were identified using LEfSe analysis to further characterize phenotypic changes in the taxonomic composition. IBD biomarker strains, including *Escherichia* and *Ruminococcus* were used as the core microbes in the Con group, while *Bacteroides* were used as the core microbe in the Bu group (LDA > 4.0; Fig. S2C).

PICRUST2-dependent prediction of microbial function, significant differences in 40 microbiota characteristic pathways between Bu and Con were identified (Table S2). Furthermore, diseases pathways, including pathogenic *Escherichia coli* infection, salmonella infection, huntington disease, *Vibrio cholerae* infection and pathways in cancer, were significantly downregulated in the Bu group compared with the Con group (Fig. S2D). Similarly, many key lipid metabolic pathways, such as ether lipid metabolism, alpha-Linolenic acid metabolism, arachidonic acid metabolism and glycerophospholipid metabolism,

were significantly downregulated in the Bu group compared with the Con group (Fig. 2G). These results indicate that *B. uniformis* can reshape the colonic microbial composition of mice with DSS-induced colitis. *B. uniformis* can also induce potential synergistic probiotics to suppress the abundance of pathogenic bacteria and may modulate the expression of colonic lipid metabolism pathways, thus alleviating colitis.

B. uniformis JCM5828 alters colonic bile acid profile in mice with DSS-induced colitis

A total of 219 and 61 differential metabolites (DEs) were identified when comparing NC *vs.* Con and Con *vs.* Bu groups, respectively (Fig. 3A), of which 117 and 52 DEs were upregulated in the NC *vs.* Con and Con *vs.* Bu groups, respectively (Fig. 3A). Although DSS treatment significantly reduced the concentration of 23-Nordeoxycholic acid, Ursodeoxycholic acid and Hyodeoxycholic acid (HDCA) in the colon of mice, whereas Bu treatment significantly restored the above concentrations (Fig. 3B). Further analysis showed that two primary bile acids (alpha-Muricholic acid (α-MCA) and isochodeoxycholic (isoCDCA)) ($P < 0.01$, Fig. 3C) and five secondary bile acids (7-ketolithocholic acid, 12-ketolithocholic acid, apocholic acid, 3-Epideoxycholic acid, and isolithocholic acid (isoLCA)) were significantly increased in the Bu group compared with the Con group ($P < 0.05$, Fig. 3C). The KEGG enrichment analysis and differential abundance (DA) score analysis were also conducted. Results showed that Bu treatment significantly up-regulated fatty acid degradation pathway (DA = 1) and down-regulated disease-related pathway of human cytomegalovirus infection, rheumatoid arthritis, human papillomavirus infection, Leishmaniasis, and amoebiasis (DA = -1; Fig. S3A). These results further confirm that the genome of *B. uniformis* strains may contain genes that can regulate bile acid metabolism.

Genomic perspective of B. uniformis transforms bile acid salts

The number of single-cell clones of Bu strains in media with different bile salt concentrations was determined to show the bile salt tolerance of Bu. The Bu strain survived up to 76.79% when 0.5% bile salt was added to the medium (Fig. S3B). It was found that the genome of *B. uniformis*[CL03T12C37] (4.9 Mb) could encode critical enzymes involved in primary bile acid biosynthesis in lipid metabolism pathway[16] (Fig. 4A). On the Bu chromosome (46% GC content in nucleobase, accession number: CP072255.1), we found via annotation that gene 1300 encodes for choloylglycine hydrolase (BSH, EC:3.5.1.24), which hydrolyzes liver-derived conjugated bile acids (CBA) to unconjugated bile acids (UCBA) and glycine or taurine [17,18] (Fig. 4B). Otherwise, the 7α-hydroxy steroid dehydrogenase (7α-HSDH), crucial for HDCA biosynthesis by αMCA, was not identified via annotation on the Bu chromosome. These results confirmed that *B. uniformis* may participate in the regulation of colonic bile acid metabolism.

B. uniformis JCM5828 alters colonic transcriptome profile in mice with DSS-induced colitis

A total of 115.66 Gb of data were obtained during RNAseq using 15 colonic epithelial samples from Bu and Con groups, which contained 511 differentially expressed genes (DEGs), of which 223 DEGs were up-regulated, and 288 DEGs were down-regulated in colonic epithelium of Bu mice compared to Con group (Fig. 5A). The typical inflammatory chemokines, including *Ccl4*, *Ccl3*, *Cxcl2*, *Cxcl3* and *Cxcr2*, can induce

immune cells to enter the site of infection during the immune response. Furthermore, *S100A8* and *S100A9* can activate inflammatory cells through neutrophil chemotaxis, and are strongly associated with various tumor diseases. In this study, the expression of *Ccl4, Ccl3, Cxcl2, Cxcl3, Cxcr2, S100A8* and *S100A9* were significantly decreased in the Bu group compared to Con group. In addition, the expression of *Ptgs2, MMp9*, and the interleukin-1 family *Il1b, Il1r2, Il1rl1, Il1f9* was significantly decreased in the Bu group compared to Con group (Fig. 5B, Table S3). In contrast, the expression of genes associated with lipid metabolism in the PPAR pathway, including ketogenic *Hmgcs2*, adipogenic *Scd1, Acaa1b, Adipoq*, and *Fabp6* was significantly increased in the Bu group compared to Con group. These genes can affect fatty acid oxidation, adipocyte differentiation, and fatty acid binding (Fig. 5B, Table S3). KEGG pathway analysis showed that most DEGs (*Mmp9, Lcn2, Il1b, Cxcl3, Ptgs2, Csf3, S100a8, S100a9, Cxcl2)* were primarily involved in intracellular inflammatory signaling pathways, including IL-17 signaling pathway and NF-κB signaling pathway (Fig. 5C). According to the established 2-way orthogonal partial least squares (O2PLS) model based on the all DEGs and DEs, nine key metabolites, especially including alpha-Muricholic acid, Isochodeoxycholic acid, and Isolithocholic acid were involved in modulated colonic epithelial gene expression (Fig. S3C). These results suggest that *B. uniformis* can ameliorate the development of DSS-induced colitis by regulating TH17 differentiation.

B. uniformis JCM5828-mediated αMCA inhibits TH17 differentiation

Herein, immunohistochemical staining of TH17 cells in mouse colon tissue was conducted to reveal whether Bu-mediated bile acids exert immunological effects by inhibiting TH17 cell differentiation. Compared with the Con group, Bu treatment significantly inhibited TH17 differentiation in the colonic lamina propria ($P < 0.001$, Fig. 6A-B). The co-culturing of Bu with LPS-treated lymphocytes from the lamina propria of the colon did not promote TH17 cell differentiation ($P > 0.05$, Fig. 6C-D), whereas addition of bile acids α-MCA, HDCA and isoLCA to lymphocytes *in vitro* significantly inhibited the differentiation of TH17 cells but isoCDCA addition had no effect whatsoever ($P < 0.001$, Fig. 6E-F). These results confirm that *B. uniformis*-mediated α-MCA and downstream secondary bile acids can inhibit TH17 differentiation, thus modulating the colonic immune response.

B. uniformis JCM5828 alleviates inflammation by inhibiting the NF-κB and MAPK signaling pathways activation

RNA-Seq data highlighted that the IL-17 and NF-κB signaling pathways were the most important inflammatory signaling pathways in the Bu group. IL-17 receptor (IL-17R) can activate downstream NF-κB, mitogen-activated protein kinase (MAPK) and other signaling pathways via the signaling complex IL-17R-Act1-TRAF6 [19] (Fig. S4). Western blot analysis of key proteins of NF-κB and MAPK signaling pathway in mouse colon tissue found that the ratios of p-NF-κB/NF-κB, p-IκB/IκB and p-IKK/IKK were significantly decreased in the Bu group ($P < 0.001$, Fig. 6G). Consistently, the MAPK pathway was significantly decreased in terms of extracellular signals related to kinases (ERK1/2), Jun amino-terminal kinases (JNK1/2) and p38 of MAPK protein family ($P < 0.05$, Fig. 6G). Overall, these results suggest that *B. uniformis* can regulate α-MCA, HDCA and isoLCA concentrations in the colon, inhibiting TH17

differentiation in colonic epithelial and the expression of downstream NF-κB and MAPK signaling pathways, thus alleviating DSS-induced colitis (Fig. 7).

Discussion

In this study, *B. uniformis* JCM5828 strain changed the colonic microbial composition and bile acid profile, especially key metabolites (αMCA, HDCA and isoLCA) that act as immune signaling molecules, thereby alleviating chronic colitis (Fig. 7). It has shown that long-term treatment of mice with *B. uniformis* CECT 7771 can alter the gut microbial composition and promote the proliferation of potentially beneficial bacteria [20,21]. *B. uniformis* CECT 7771 can enhance the activity of macrophages and dendritic cells (DCs), restore the ability of DCs to recognize antigens and stimulate the proliferation of T lymphocytes [20]. *B. uniformis* CECT 7771 can also reduce serum cholesterol, triglyceride, glucose and insulin levels in obese mice, and the number of fat particles in the small intestine, thus alleviating the metabolic and immune disorders caused by high-fat diets [22]. DSS can induce colon epithelial damage and promote the proliferation of harmful bacteria causing diarrheal phenotypes in animals [23]. Several studies have shown that Th17 cells are involved in the pathogenesis of DSS-induced colitis [24,25]. Mucus layer thickness can be used to assess the function of the intestinal barrier and protect the epithelium from harmful factors [26]. The tight junction protein can effectively prevent the paracellular transport of bacteria, toxins and other substances in the intestinal lumen through regulation, thus maintaining the integrity of the epithelial barrier function of the intestinal mucosa [27,28]. According to the present study, *B. uniformis* could alleviate the impaired colonic mucosal immune barrier induced by DSS and inhibited anti-inflammatory cytokine genes, thus triggering Th17 response.

Previous studies have demonstrated IBD development is associated with gut microbiota [29,30]. Some functional strains used for IBD treatment rely on their probiotic functions. For example, the *Gassericin A bacteriocins* secreted by *L gasseri* LA39 and *L frumenti* can up-regulate intestinal fluid absorption-related proteins and improve intestinal epithelial barrier function in early weaned piglets by interacting with the host KRT19 protein [31]. *Akkermansia muciniphila* secrets a P9 protein that induces the secretion of glucagon-like peptide-1 (GLP-1), thus ameliorating glucose homeostasis and metabolic diseases in mice [32]. However, most strains in the gut induce probiotic effects by disrupting the composition of the intestinal microbes and synergizing with some of the original intestinal strains, thus affecting the metabolites. For example, the microbiota-associated metabolites taurine, histamine, and spermine can ameliorate colitis via synergistic regulation of NLRP6 inflammasome signaling, epithelial IL-18 secretion, and downstream anti-microbial peptide (AMP) profiles, thus restoring normal microbiota [33]. In this study, *B. uniformis* induced anti-inflammatory function in the intestine mainly by synergizing with other gut strains, including *Bifidobacterium*, *Bacteroides*, and *Lactobacillus*, thus altering the colonic bile acid profile and suppressing the abundance of *Ruminococcus* and *Escherichia shigella* pathogenic bacteria. Previous studies have shown that some *Bifidobacteria* and *Lactobacillus* have an anti-inflammatory function. For instance, *Bifidobacterium pseudolongum* can improve the human immune response, prevent intestinal diseases, inhibit allergies and lower cholesterol [34]. *Lactobacillus vaginalis* can produce

various bacteriocins, such as acidolin, acidophilin and laetocidon, thus preventing the growth of pathogenic microorganisms due to its good antibacterial effect [35]. *Ruminococcus-gnavus* secretes glucorhamnan, a complex polysaccharide with rhamnose skeleton and glucose side chain, that can effectively induce dendritic cells to secrete inflammatory cytokines (TNF-α), thus leading to colitis development [36]. Excess *Ruminococcus* is a key indicator of irritable bowel syndrome (IBS) [37]. *Escherichia-Shigella* is an adherent-invasive bacterium whose abundance increases in the UC group, thus aggravating colitis development [38].

Genomic sequencing also showed that the gene encoding BSH in *B. uniformis* is involved in UCDA biosynthesis in the host colon [18]. Furthermore, both sterile mice and antibiotic treatment significantly increased CBA accumulation in the intestinal cavity and significantly decreased the level of secondary bile acids [39]. In addition, colonized BSH knockout *B. thetaiotaomicron* significantly affected bile acid metabolism of the host in sterile mice [40]. Results further showed that BSH of *B. uniformis* participates in α-MCA biosynthesis. However, *B. uniformis* does not contain the gene that converts α-MCA to the corresponding secondary bile acids [41–43]. Therefore, *B. uniformis* regulates the biosynthesis of secondary bile acid by regulating the structure of gut microbiota through other functional strains. Nevertheless, host enzyme may be involved in this process. In addition, bicyclol reduces liver injury in mice by increasing the levels of α-MCA, regulating bile acid metabolism and improving histopathological parameters [44]. However, it is unknown whether α-MCA can alleviate inflammation through TH17 cells. HDCA can improve intestinal bile acid profile and induce anti-inflammatory effects in mice by inhibiting intestinal proinflammatory factor production in the bile acid receptor (FXR) [45]. The isoLCA inhibits TH17 differentiation by binding and inhibiting the transcriptional activity of RORγt. Furthermore, colonization of mice with enterobacteria producing isoLCA decreases TH17 cells [46], thus secreting proinflammatory cytokines, exacerbating pathogen invasion and decreasing host immunity [47,48]. However, our studies reveal *B. uniformis* to directly mediate α-MCA and indirectly mediate HDCA and isoLCA in mice, thereby inhibiting TH17 cell differentiation and thus modulating the intestinal immune response. Therefore, metabolites from the gut microbiota can mediate the complicated interaction between the gut microbiota and the host.

IL-17 and NF-κB are the most important inflammatory signaling pathways [49,50]. Interaction of both pathways amplify inflammatory signals via the MAPK pathway. Receptor proteins in the inflammatory pathway can regulate gene transcription and expression by binding to promoter and enhancer sequence sites of various proinflammatory genes, thereby exacerbating the inflammatory response [51,52]. NF-κB dimers are sequestered in the cytosol of unstimulated cells via interactions with their inhibitor molecule IκB. IκB can be phosphorylated after lipopolysaccharide stimulation, leading to the release of NF-κB. Furthermore, phosphorylated NF-κB translocates to the nucleus and activates cytokine expression [51]. The MAPK signaling pathway is shared by four distinct cascades (ERK1/2, JNK1/2/3, p38-MAPK, and ERK5) [53,54]. However, the role of ERK in inflammation is controversial. Some studies have found that decreased ERK can suppress inflammation [55,56], while other studies have reported that the ERK activation can

protect against inflammation [57]. These results demonstrate that *B. uniformis* can significantly suppress the phosphorylation of IκK (the IκB kinase), IκB, NF-κB, ERK1/2, JNK1/2, and p38-MAPK, thus relieving inflammation. Therefore, *B. uniformis* mediated α-MCA and downstream secondary bile acids to alleviate inflammation by inhibiting the NF-κB and MAPK signaling pathways activation.

Conclusion

In this study, gut microbe-metabolite could control host immune responses by directly modulating immune cells. TH17 cells have critical roles in various inflammatory diseases and are closely associated with gut-residing bacteria. In this study, novel modulatory pathways that can regulate T cell function through microbe-mediated bile acid metabolites were identified. Bile acids molecules can regulate host physiology and immune responses, indicating that understanding the role of host-microbiota networks in mediating bile acids biotransformations can provide therapeutic interventions for IBD diseases. However, future studies should elucidate the *B. uniformis* or host enzymes that generate α-MCA for effective control of T cell function in the context of autoimmune diseases and other inflammatory conditions.

Methods

Isolation of B. uniformis JCM5828 using culture-based techniques

The *B. uniformis* JCM5828 strain was isolated from the feces of healthy goat kids. Briefly, the feces were transferred to a 5 mL sterile cryopreservation tube containing 30% glycerol immediately after collection, and stored at -80°C after snap-freezing in liquid nitrogen. Each 1g of feces per sample were suspended in PBS buffer and diluted by a gradient up to 10^{-8}. Then, 0.01‰ heme chloride (16009-13-5, Yuanye, China), 0.01‰ vitamin K1 (84-80-0, Sangon, China), 0.1‰ kanamycin (8063-07-8, bidepharm, China), 0.0075‰ vancomycin (1404-90-6, Macklin, China), and 5% defibrinated sheep blood (TX0030, Solarbio, China) were added to the original Brucella Broth medium (LA3560, Solarbio, China) to form improved Brucella Broth medium. The sample (50 μL) was used to coat the solid medium, then anaerobically cultured at 37°C for 48 h. Single colonies were then selected for species identification and target strains were obtained.

DNA extraction and bacteria quantification

TIANamp Bacterial DNA Kit (DP302-02, Tiangen, Chian) was used to extract genomic DNA of *B. uniformis JCM5828*. The 16S rDNA was amplified via PCR (Full-gold (Beijing, China) 2×EasyTaq PCR SuperMix) using the following reaction primers: forward primers: 5 '- AGAGTTTGATCCTGGCTCAG – 3', reverse primers: 5 '- TACGGYTACCTTGTTACGACTT – 3'. The extracted DNA samples were diluted and used as PCR template. The amplified PCR products were then subjected to agarose gel electrophoresis, and the prepared PCR products were sent to AuGCT DNA-SYN Biotechnology Co., Ltd. (Beijing, China) for sequencing.

Preparation of B. uniformis JCM5828

Purified *B. uniformis* JCM5828 was cultured anaerobically at 37°C for 24h, then 50 mL of cultured liquid was centrifuged at 12,000 * *g*, and 4°C for 10 min. The supernatant was discarded, while the sample was washed with PBS and suspended with normal saline for gradient dilution to adjust the concentration of *B. uniformis* JCM5828 for subsequent intragastric treatment.

Experimental animals

A total of 24 female C57BL/6 mice of 8 weeks of age were purchased from Chongqing Tengxin Biotechnology Co., Ltd. (Xi'an, China). The mice were kept in the Animal Experiment Center of Northwest A&F University under SPF conditions, ambient temperature 23 ± 1°C, humidity 55 ± 5% and pathogen-free conditions on a 12/12 h light/dark cycle with free access to food and water. Diet composition and nutritional value are shown in Table S4. The experiment was approved by the Institutional Animal Care and Use Committee of the Northwest A&F University (permit number; 2021-06-008).

Chronic colitis model and treatments

The mice were given drinking water containing 3.0% (wt/vol) DSS (MP Biomedicals, Santa Ana, CA, US, molecular weight of 36,000−50,000) for 24 days to establish colitis model. The mice in the Bu group (DSS + Bu) were given 1×10^9 CFU of *B. uniformis* JCM5828 suspended in 200 μl sterile anaerobic PBS via oral gavage on the 15th day, while mice in the Con group (DSS + PBS) were given an equivalent volume of sterile anaerobic PBS. The mice in the NC group were given drinking water throughout the whole course and equivalent volume of sterile anaerobic PBS was given intragastric administration on day 15. The treatment was continued for 10 days. Body weight, food intake and diarrhea scores were recorded each day. The diarrhea score was determined according to the previous standard procedure [58]. Rectal bleeding scores were as follows: 0 = normal colored stool, 1 = brown stool, 2 = reddish stool and 3 = bloody stool; diarrhea: 0 = well-formed stools, 1 = mildly soft stool, 2 = very soft stool and 3 = watery stools.

Tissue collection, fixation and histochemistry

The colon samples were fixed in 4% polyformaldehyde, embedded in paraffin, sectioned, and stained with hematoxylin and eosin (H&E) for pathological analysis. Two independent investigators blinded to the treatment evaluated the slides. The inflammatory infiltrate, goblet cell loss, crypt density, muscle thickening, submucosal inflammation, crypt abcess and ulcerations were described using a 0−4 point scale according to the previous standard procedure [59]. Immunohistochemistry was performed using primary antibodies of rabbit anti-IL17A (eBio17B7, eBioscience™, US), visualized using 3,3'-diaminobenzidine (DAB) and counterstained using hematoxylin. Image J software (National Institutes of Health, Bethesda, Maryland) was used to determine the cell numbers.

RNA extraction and quantitative real-time PCR

TRIzol Reagent (Cwbio, China) was used to extract RNA from the colon tissues. The total RNA was then reverse transcribed using RevertAid First Strand cDNA Synthesis Kit (Thermo, US) to obtain cDNA. qRT-

PCR was performed using ChamQ Universal SYBR qPCR Master Mix (Vazyme, China) in the Light Cycler®96 Real-Time PCR System (Roche, US). All primers used in this study were designed and preliminarily verified using Oligo 7 software and Primer-BLAST (https://www.ncbi.nlm.nih.gov/tools/primer-blast/). The primers were synthesized in Zhongke Yutong (Xi 'an, China) Company (Table S5). The comparative cycle method (2 − ΔΔCt) was used to determine the relative mRNA expression.

DNA isolation and PCR amplification and sequencing

E.Z.N.A Stool DNA Kit (Omega Bio-tek, Norcross, GA, US) was used to extract DNA from 24 stool samples following the kit's operating instructions. A Nanodrop 2000 UV-VI spectrophotometer (Thermo Scientific, Wilmington, US) was used to determine the concentration and purity of the extracted DNA, while 1% agarose gel electrophoresis was conducted to assess the DNA quality. Amplification was then performed using primers 338F (5'-ACTCCTACGGGAGGCAGCAG-3') and 806R (5'-GGACTACHVGGGTWTCTAAT-3') targeting the V3-V4 16S rDNA region. Finally, the purified amplicons were combined into equimolar ratios for up-sequencing. The sequencing was performed by Majorbio BioTech Co. (Shanghai, China).

16S rRNA gene data analysis

The analysis is described online at the Majorbio Cloud Platform (www.majorbio.com) [60]. Briefly, the sequences were multiplexed using FLASH software (version 1.2.7), then double-ended reads were merged using FASTP software version 0.19.6) [61]. The sequences were then filtered, denoised, merged and chimeras removed using the DADA2 plugin in the QIIME2 platform [62]. The number of reads per sample was pumped flat to 23,400 to minimize the effect of sequencing depth on alpha and beta diversity analysis. Finally, the data achieved an average Good coverage of 99.83%. Amplicon sequence variants (ASVs) were assigned for classification using the naive Bayes consensus taxonomy classifier for SILVA 138/16s_bacteria in QIIME2.

RNA-Seq analysis

Extraction of total RNA from tissue samples and testing of the concentration and purity of the extracted RNA using Nanodrop2000. RNA-Seq was performed by Majorbio BioTech Co., Shanghai, China. The Illumina Novaseq 6000 platform was used to construct RNA libraries and generate reads of 300 bp long paired-end (Illumina, San Diego, CA). The read number of each gene was transformed into FPKM (fragment per kilobase of exon model per million mapped reads). The differentially expressed genes were identified using the DEGseq2 package [63]. KEGG pathway enrichment analysis of the DEGs was performed using the KOBAS software [64].

Immunofluorescence staining

The sections of paraffin-embedded tissue were stained with ZO-1 antibody (ab221547, Abcam, UK), Claudin-1 antibody (ab211737, Abcam, UK) and DAPI (C0060, solarbio, China) for immunofluorescence. Two investigators blinded to the treatment independently evaluated the slides. SlideViewer 2.5.0

(3DHISTECH Ltd., Hungary) was used for imaging while Image J software (National Institutes of Health, Bethesda, Maryland) was used to analyze the fluorescence signal intensity.

Western blot analysis

Colon tissues were weighed and homogenized in Cell lysis buffer (Beyotime, China). The homogenate was then centrifuged at at 15,000 g and 4°C for 15 min to obtain the supernatant. Omni-Easy™ instant BCA protein assay kits (Epizyme, China) were used to quantify protein concentration following the manufacturer's instructions. The proteins were separated using 10% SDS polyacrylamide gel, then transferred onto PVDF membranes. The membranes were blocked with 5% skimmed milk for 1 h, then immunoblotted with primary antibodies against IKK-α (ab32041, Abcam, UK), Phospho-IKKα/β (Ser176/180) (#2697, CST), IKB-α (ab32518, Abcam, UK), IKB-α (phospho S36) (ab133462, Abcam, UK), NF-κB p65 (#8242, CST, US), NF-κB p65(phospho Ser536) (ab76302, Abcam, UK), p38 MAPK (#8690, CST, US), Phospho-p38 MAPK (Thr180/Tyr182) (#4511, CST, US), p44/42 MAPK (#4695, CST, US), p-p44/42 MAPK (#4370, CST, US), SAPK/JNK (#9252, CST, US), p-SAPK/JNK (#4668, CST, US), GAPDH (#5174, CST, US) at 4°C overnight. The membranes were washed three times with 1x TBST (T1081, Solarbio, China) for 5 minutes each time, then incubated with second antibodies labeled with HRP at room temperature for 1h. The bands were visualized using Omni-ECL™pico light chemiluminescence kits (Epizyme, China). GAPDH was used as a reference protein.

Bile tolerance

Bile salts were added to BHI liquid medium (mass concentration; 0, 0.1, 0.3 and 0.5 g/100 mL) into test tubes. The tubes were autoclaved at 121 °C for 20 min, then cooled to room temperature. The activated *Bu* was inoculated with 5% inoculum into the above medium. The OD600 value of each group was measured after 24 h of anaerobic static culture at 37 °C. Survival rate was calculated as follows: (N1/N0) × 100%. N1 (log CFU/ml) was described as the total viable count of selected strains after treatment, while N0 (log CFU/ml) represents the total viable count of selected strains before treatment. CFU represents colony-forming unit [65].

Comparative genomics

The genome sequence of *B.uniformis*[CL03T12C37] data retrieved from GenBank (*B.uniformis* CL03T12C37 (ID 994) - genome - NCBI (nih.gov)), were uploaded to the Type (Strain) Genome Server (TYGS), Majorbio BioTech platform (Shanghai, China), for a whole genome-based taxonomic analysis.

Metabolomics data collection and processing

The samples were processed as follows. First, 16 frozen samples were thawed on ice, then about 50 mg of the sample was put into a 2 ml centrifuge tube, and the true sample mass was recorded. Methanol internal standard solution (500 μL, 70%) was added to the sample and vortexed for 3 min, then allowed to stand in a -20°C refrigerator for 30 min. The liquid was placed in a centrifuge, then centrifuged at 12000 r/min and 4°C for 10 min. Supernatant (250 μl) was aspirated and placed in a centrifuge, then centrifuged at 12000 r/min and 4°C for 5 min. The centrifuged supernatant (150 μl) in the injection bottle was also

aspirated. Qualitative analysis was performed using the MWDB (metware database) based on the retention time (RT) of the test substance, information of daughter ion pair and secondary spectral data of the test substance.

Isolation of lamina propria lymphocytes

The intestines were cut open and rinsed using ice-cold PBS to isolate the colon lamina propria cells. Associated fats were carefully removed and incubated in prewarmed 1× HBSS (at 37°C for 40 min) (without calcium and magnesium) containing 1 mM dithiothreitol, 5 mM EDTA and 1% fetal bovine serum (FBS) in a shaking incubator. The tissues were then rinsed with warm RPMI (at 37°C for 1 h) containing 50 µg ml^{-1} Liberase D, 50 µg ml^{-1} DNase I and 1% FBS) to remove excess EDTA and digestion medium in a shaking incubator. Mononuclear cells were collected at the interface of a 40%/80% Percoll gradient (Solarbio, China). The cells were washed twice using PBS and counted. The test was continued if the cell viability was above 95%.

In vitro T cell culture

Native T cells were isolated from the colon lamina propria of C57BL/6 mice (aged 6 to 8 weeks) via FACS sorting. Then, 96-well flat-bottom plates were precoated with 50 µl of anti-CD3e (145-2C11, Thermo, US, 0.25 µg ml – 1) antibodies at 37°C for 2 h. The naive CD4$^+$ T cells (1×10^6) were seeded into T cell medium (RPMI supplemented with 10% fetal bovine serum, 25 mM glutamine, 55 µM 2-mercaptoethanol, 100 U ml^{-1} penicillin, 100 mg ml^{-1} streptomycin) after multiple washes with 1× DPBS. Their T cell receptor downstream signaling pathways (TCR activation) were activated with soluble anti-CD28 (13-0281-82, Thermo, US, 2 µg ml^{-1}) antibodies. IL-6 (200-06, Peprotech, US, 20 ng ml^{-1}) and human TGF-β1 (100 – 21, Peprotech, US, 0.3 ng ml^{-1}) were added to the sample for TH17 cell differentiation. The cells were cultured at 37°C for 2−4 days to increase the final yield.

Cell culture and treatment

Bacterial supernatants, α-Muricholic acid (2393-58-0, Macklin, China), Isochenodeoxycholic acid (566-24-5, Leyan, China), Hyodeoxycholic acid (83-49-8, Sigma-Aldrich, US) and isolithocholic acid (1534-25-6, Yuanye, China) were added to the sample after TCR activation. The T cells were then cultured at 37°C in humidified 5% CO^2 atmosphere. The bacterial supernatant was collected via centrifugation (12,000 * g, 10 min). The bile acids were dissolved in DMSO, then added to T cells through a 0.2 µm filter for co-culture for three days. Finally, flow cytometry was used to analyze the percentage of Th17 cells.

Flow cytometry

The cells were stained with various surface marker antibodies supplemented with LIVE/DEAD Fixable dye (L23105, Thermo, US) for dead cell exclusion after co-cultivation. The cells were washed with flow cytometry staining buffer (00-4222-26, Thermo, US), then fixed, permeabilized with the fixation and permeabilization solution (554722, BD eBiosciences, US) and intracellularly stained to determine the cytokines factors. The following antibodies were used at the indicated dilutions for staining: anti-Foxp3

(1:100, 17-5773-80, eBiosci-ence, US), anti-RORγt (1:100, 562607, BD Biosciences, US). The samples were analyzed using a Flow Cytometer (BD Biosciences, US). FlowJ software (Tree Star Inc., San Carlos, CA) was used for subsequent analyses.

Statistical analysis

Data were expressed as mean ± SEM. Unpaired Student's test, Mann−Whitney U test, one-way ANOVA test and Kruskal−Wallis test were used to analyze the data. Wilcoxon rank sum tests were used to compare colonic contents alterations in different groups. Wilcoxon rank sum test was also used to analyze differences in alpha diversity and predicted pathway abundances. A p-value threshold of 0.05 (Wilcoxon rank sum test) and an effect size threshold of 2 were used for all bacterial taxa. A P value < 0.05 was considered statistically significant. GraphPad Prism 9.0.0 software (GraphPad Software, Inc., La Jolla, CA, US) and SPSS 25.0 for Windows (SPSS Inc., Chicago, IL, US) were used for all statistical analyses.

Declarations

Ethics approval and consent to participate

The experiment was approved by the Institutional Animal Care and Use Committee of the Northwest A&F University under permit number 2021-06-008.

Consent for publication

Not applicable.

Availability of data and material

The samples of 16S rRNA gene sequencing was available from the NCBI under accession PRJNA 911642, and RNA-Seq sequencing was available from the NCBI under accession PRJNA912399.

Competing interests

The authors declare that they have no competing interests.

Funding

Authors' contributions

Enping Zhang: Conceptualization, Project administration, Writing - review & editing, Funding acquisition. **Yiting Yan:** Conceptualization, Methodology, Investigation, Visualization, Supervision, Writing

References

1. Ye, L., Cao, Q. & Cheng, J. Review of inflammatory bowel disease in China. The Scientific World Journal **2013** (2013).

2. Ng, S. C. *et al.* Geographical variability and environmental risk factors in inflammatory bowel disease. Gut **62**, 630–649 (2013).

3. Molodecky, N. A. *et al.* Increasing incidence and prevalence of the inflammatory bowel diseases with time, based on systematic review. *Gastroenterology* **142**, 46–54. e42 (2012).

4. Chen, Y. *et al.* Probiotic mixtures with aerobic constituent promoted the recovery of multi-barriers in DSS-induced chronic colitis. Life sciences **240**, 117089 (2020).

5. Ray, K. Human faecal sample processing in metagenomic studies: striving for standards. Nature Reviews Gastroenterology & Hepatology **14**, 631–631 (2017).

6. Parada Venegas, D. *et al.* Short chain fatty acids (SCFAs)-mediated gut epithelial and immune regulation and its relevance for inflammatory bowel diseases. Frontiers in immunology, 277 (2019).

7. Chiang, J. Y. & Ferrell, J. M. Bile acid receptors FXR and TGR5 signaling in fatty liver diseases and therapy. American Journal of Physiology-Gastrointestinal and Liver Physiology **318**, G554-G573 (2020).

8. Bornet, E. & Westermann, A. J. The ambivalent role of Bacteroides in enteric infections. Trends in Microbiology **30**, 104–108 (2022).

9. Imdahl, F. & Saliba, A.-E. Advances and challenges in single-cell RNA-seq of microbial communities. Current Opinion in Microbiology **57**, 102–110 (2020).

10. Bousbaine, D. *et al.* A conserved Bacteroidetes antigen induces anti-inflammatory intestinal T lymphocytes. Science **377**, 660–666 (2022).

11. Gul, L. *et al.* Extracellular vesicles produced by the human commensal gut bacterium Bacteroides thetaiotaomicron affect host immune pathways in a cell-type specific manner that are altered in inflammatory bowel disease. Journal of Extracellular Vesicles **11**, e12189 (2022).

12. Lee, Y. K. *et al.* The protective role of Bacteroides fragilis in a murine model of colitis-associated colorectal cancer. MSphere **3**, e00587-00518 (2018).

13. Zhang, K. *et al.* Gut microbiota-derived metabolites contribute negatively to hindgut barrier function development at the early weaning goat model. Animal Nutrition (2022).

14. Singh, R. P., Rajarammohan, S., Thakur, R. & Hassan, M. Linear and branched β-Glucans degrading enzymes from versatile Bacteroides uniformis JCM 13288T and their roles in cooperation with gut bacteria. Gut microbes **12**, 1826761 (2020).

15. López-Almela, I. *et al.* Bacteroides uniformis combined with fiber amplifies metabolic and immune benefits in obese mice. Gut Microbes **13**, 1–20 (2021).

16. García-Bayona, L., Coyne, M. J. & Comstock, L. E. Mobile Type VI secretion system loci of the gut Bacteroidales display extensive intra-ecosystem transfer, multi-species spread and geographical clustering. PLoS genetics **17**, e1009541 (2021).

17. Dey, N. *et al.* Regulators of gut motility revealed by a gnotobiotic model of diet-microbiome interactions related to travel. Cell **163**, 95–107 (2015).

18. Núñez-Sánchez, M. A. *et al.* Microbial bile salt hydrolase activity influences gene expression profiles and gastrointestinal maturation in infant mice. Gut microbes **14**, 2149023 (2022).

19. Qu, F. *et al.* TRAF6-dependent Act1 phosphorylation by the IκB kinase-related kinases suppresses interleukin-17-induced NF-κB activation. Molecular and cellular biology **32**, 3925–3937 (2012).

20. Gauffin Cano, P., Santacruz, A., Moya, Á. & Sanz, Y. Bacteroides uniformis CECT 7771 ameliorates metabolic and immunological dysfunction in mice with high-fat-diet induced obesity. (2012).

21. Gómez del Pulgar, E. M., Benítez-Páez, A. & Sanz, Y. Safety assessment of bacteroides uniformis CECT 7771, a symbiont of the gut microbiota in infants. Nutrients **12**, 551 (2020).

22. Fabersani, E. *et al.* Bacteroides uniformis CECT 7771 alleviates inflammation within the gut-adipose tissue axis involving TLR5 signaling in obese mice. Scientific reports **11**, 1–15 (2021).

23. Chassaing, B., Aitken, J. D., Malleshappa, M. & Vijay-Kumar, M. Dextran sulfate sodium (DSS)-induced colitis in mice. *Current protocols in immunology* **104**, 15.25. 11-15.25. 14 (2014).

24. Yu, R., Zuo, F., Ma, H. & Chen, S. Exopolysaccharide-producing Bifidobacterium adolescentis strains with similar adhesion property induce differential regulation of inflammatory immune response in Treg/Th17 axis of DSS-colitis mice. Nutrients **11**, 782 (2019).

25. Cheng, C. *et al.* Hyperoside ameliorates DSS-induced colitis through MKRN1-mediated regulation of PPARγ signaling and Th17/Treg balance. Journal of Agricultural and Food Chemistry **69**, 15240–15251 (2021).

26. Rupani, B. *et al.* Relationship between disruption of the unstirred mucus layer and intestinal restitution in loss of gut barrier function after trauma hemorrhagic shock. Surgery **141**, 481–489 (2007).

27. Al-Sadi, R. *et al.* Interleukin-6 modulation of intestinal epithelial tight junction permeability is mediated by JNK pathway activation of claudin-2 gene. PloS one **9**, e85345 (2014).

28. Ukena, S. N. *et al.* Probiotic Escherichia coli Nissle 1917 inhibits leaky gut by enhancing mucosal integrity. PloS one **2**, e1308 (2007).

29. Fan, L. *et al.* B. adolescentis ameliorates chronic colitis by regulating Treg/Th2 response and gut microbiota remodeling. Gut Microbes **13**, 1826746 (2021).

30. Liu, C. *et al.* Cohousing-mediated microbiota transfer from milk bioactive components-dosed mice ameliorate colitis by remodeling colonic mucus barrier and lamina propria macrophages. Gut Microbes **13**, 1903826 (2021).

31. Hu, J. *et al.* A microbiota-derived bacteriocin targets the host to confer diarrhea resistance in early-weaned piglets. *Cell Host & Microbe* **24**, 817–832. e818 (2018).

32. Yoon, H. S. *et al.* Akkermansia muciniphila secretes a glucagon-like peptide-1-inducing protein that improves glucose homeostasis and ameliorates metabolic disease in mice. Nature Microbiology **6**, 563–573 (2021).

33. Levy, M. *et al.* Microbiota-modulated metabolites shape the intestinal microenvironment by regulating NLRP6 inflammasome signaling. Cell **163**, 1428–1443 (2015).

34. Bo, T.-b. *et al.* Bifidobacterium pseudolongum reduces triglycerides by modulating gut microbiota in mice fed high-fat food. The Journal of steroid biochemistry and molecular biology **198**, 105602 (2020).

35. Jespers, V. *et al.* The significance of Lactobacillus crispatus and L. vaginalis for vaginal health and the negative effect of recent sex: a cross-sectional descriptive study across groups of African women. BMC infectious diseases **15**, 1–14 (2015).

36. Henke, M. T. *et al.* Ruminococcus gnavus, a member of the human gut microbiome associated with Crohn's disease, produces an inflammatory polysaccharide. *Proceedings of the National Academy of Sciences* **116**, 12672–12677 (2019).

37. Danilova, N. *et al.* Markers of dysbiosis in patients with ulcerative colitis and Crohn's disease. Terapevticheskii arkhiv **91**, 13–20 (2019).

38. Zhang, Z. *et al.* A diversified dietary pattern is associated with a balanced gut microbial composition of Faecalibacterium and Escherichia/Shigella in patients with Crohn's disease in remission. Journal of Crohn's and Colitis **14**, 1547–1557 (2020).

39. Sayin, S. I. *et al.* Gut microbiota regulates bile acid metabolism by reducing the levels of tauro-beta-muricholic acid, a naturally occurring FXR antagonist. Cell metabolism **17**, 225–235 (2013).

40. Yao, L. *et al.* A selective gut bacterial bile salt hydrolase alters host metabolism. Elife **7** (2018).

41. Jia, W., Xie, G. & Jia, W. Bile acid–microbiota crosstalk in gastrointestinal inflammation and carcinogenesis. Nature reviews Gastroenterology & hepatology **15**, 111–128 (2018).

42. Wahlström, A., Sayin, S. I., Marschall, H.-U. & Bäckhed, F. Intestinal crosstalk between bile acids and microbiota and its impact on host metabolism. Cell metabolism **24**, 41–50 (2016).

43. Funabashi, M. *et al.* A metabolic pathway for bile acid dehydroxylation by the gut microbiome. Nature **582**, 566–570 (2020).

44. Zhao, J. *et al.* Bicyclol Alleviates Signs of BDL-Induced Cholestasis by Regulating Bile Acids and Autophagy-Mediated HMGB1/p62/Nrf2 Pathway. Frontiers in Pharmacology, 1832 (2021).

45. Song, M. *et al.* Hyodeoxycholic acid (HDCA) suppresses intestinal epithelial cell proliferation through FXR-PI3K/AKT pathway, accompanied by alteration of bile acids metabolism profiles induced by gut bacteria. The FASEB Journal **34**, 7103–7117 (2020).

46. Paik, D. *et al.* Human gut bacteria produce TH17-modulating bile acid metabolites. Nature **603**, 907–912 (2022).

47. Yang, J., Sundrud, M. S., Skepner, J. & Yamagata, T. Targeting Th17 cells in autoimmune diseases. Trends in pharmacological sciences **35**, 493–500 (2014).

48. Jiang, P. *et al.* The involvement of TH17 cells in the pathogenesis of IBD. Cytokine & Growth Factor Reviews (2022).

49. Giri, R. *et al.* Secreted NF-κB suppressive microbial metabolites modulate gut inflammation. Cell Reports **39**, 110646 (2022).

50. Kim, T.-W. *et al.* Anti-Inflammatory mechanisms of Koreanaside A, a lignan isolated from the flower of Forsythia koreana, against LPS-induced macrophage activation and DSS-induced colitis mice: the crucial role of AP-1, NF-κB, and JAK/STAT signaling. Cells **8**, 1163 (2019).

51. Lan, W., Wang, Z., Liu, J. & Liu, H. Methionyl-methionine exerts anti-inflammatory effects through the JAK2-STAT5-NF-κB and MAPK signaling pathways in bovine mammary epithelial cells. Journal of agricultural and food chemistry **68**, 13742–13750 (2020).

52. Chen, X. *et al.* NEK7 interacts with NLRP3 to modulate the pyroptosis in inflammatory bowel disease via NF-κB signaling. Cell death & disease **10**, 1–12 (2019).

53. Guo, Y. J. *et al.* ERK/MAPK signalling pathway and tumorigenesis. Experimental and therapeutic medicine **19**, 1997–2007 (2020).

54. Braicu, C. *et al.* A comprehensive review on MAPK: a promising therapeutic target in cancer. Cancers **11**, 1618 (2019).

55. Huang, Y.-C. *et al.* Galangin ameliorates cisplatin-induced nephrotoxicity by attenuating oxidative stress, inflammation and cell death in mice through inhibition of ERK and NF-kappaB signaling. Toxicology and applied pharmacology **329**, 128–139 (2017).

56. Ryu, H.-H. *et al.* Excitatory neuron–specific SHP2-ERK signaling network regulates synaptic plasticity and memory. Science signaling **12**, eaau5755 (2019).

57. Khan, N. M. *et al.* Wogonin, a plant derived small molecule, exerts potent anti-inflammatory and chondroprotective effects through the activation of ROS/ERK/Nrf2 signaling pathways in human Osteoarthritis chondrocytes. Free Radical Biology and Medicine **106**, 288–301 (2017).

58. Nishiyama, Y., Kataoka, T., Yamato, K., Taguchi, T. & Yamaoka, K. Suppression of dextran sulfate sodium-induced colitis in mice by radon inhalation. *Mediators of inflammation* 2012 (2012).

59. Development of Reliable, Valid and Responsive Scoring Systems for Endoscopy and Histology in Animal Models for Inflammatory Bowel Disease. Journal of Crohn's and Colitis (2018).

60. Bolyen, E. *et al.* Reproducible, interactive, scalable and extensible microbiome data science using QIIME 2. Nature biotechnology **37**, 852–857 (2019).

61. Chen, S., Zhou, Y., Chen, Y. & Gu, J. fastp: an ultra-fast all-in-one FASTQ preprocessor. Bioinformatics **34**, i884-i890 (2018).

62. Callahan, B. J. *et al.* DADA2: High-resolution sample inference from Illumina amplicon data. Nature methods **13**, 581−583 (2016).

63. Love, M. I., Huber, W. & Anders, S. Moderated estimation of fold change and dispersion for RNA-seq data with DESeq2. Genome biology **15**, 1−21 (2014).

64. Xie, C. *et al.* KOBAS 2.0: a web server for annotation and identification of enriched pathways and diseases. Nucleic acids research **39**, W316-W322 (2011).

65. Azat, R. *et al.* Probiotic properties of lactic acid bacteria isolated from traditionally fermented Xinjiang cheese. Journal of Zhejiang University-Science B **17**, 597−609 (2016).

Figures

Figure 1
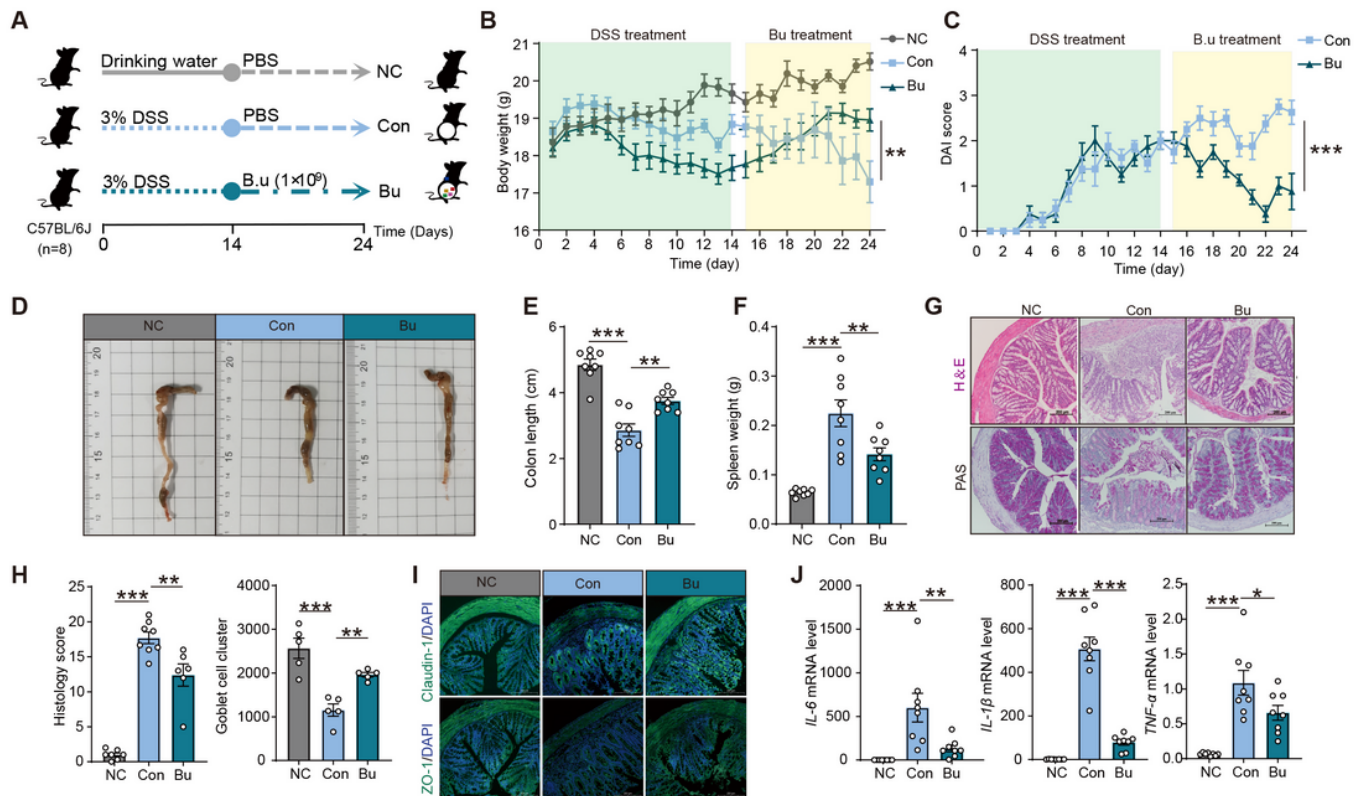
Figure 1

B. uniformis JCM5828 ameliorates DSS-induced colitis by protecting against intestinal barrier damage and tight junction disruption. (A) Schematic of the experimental design. Mice (female, *n* = 8 per group) were given 3.0% DSS for 24 days and treated with *B. uniformis* JCM5828 from day 15 to day 24. (B) Changes in body weights during the experiments. (C) DAI scores during the experiments. (D-E) Colon tissues isolated on the last day of the experiment. A representative image of colon tissue from each

group was provided, and the colon length was recorded. (F) The spleen weight of each group. (G-H) H&E and PAS staining showing the histological analysis of mouse colon tissue. Scale bar = 200 µm. Histological scores and goblet cell number of the DSS-induced colitis were evaluated (*n* = 8 per group). (I) Immunofluorescence staining showing the localization of ZO-1 and claudin-1 in the mouse colon on the last day of the experiment. Scale bar = 200 µm. (J) qPCR analysis showing the mRNA expression of *IL-6*, *IL-1β*, *TNF-α* in colon tissues. *$p < 0.05$, **$p < 0.01$, ***$p < 0.001$. Data were analyzed using one-way ANOVA and expressed as means ± SEM.

Figure 2
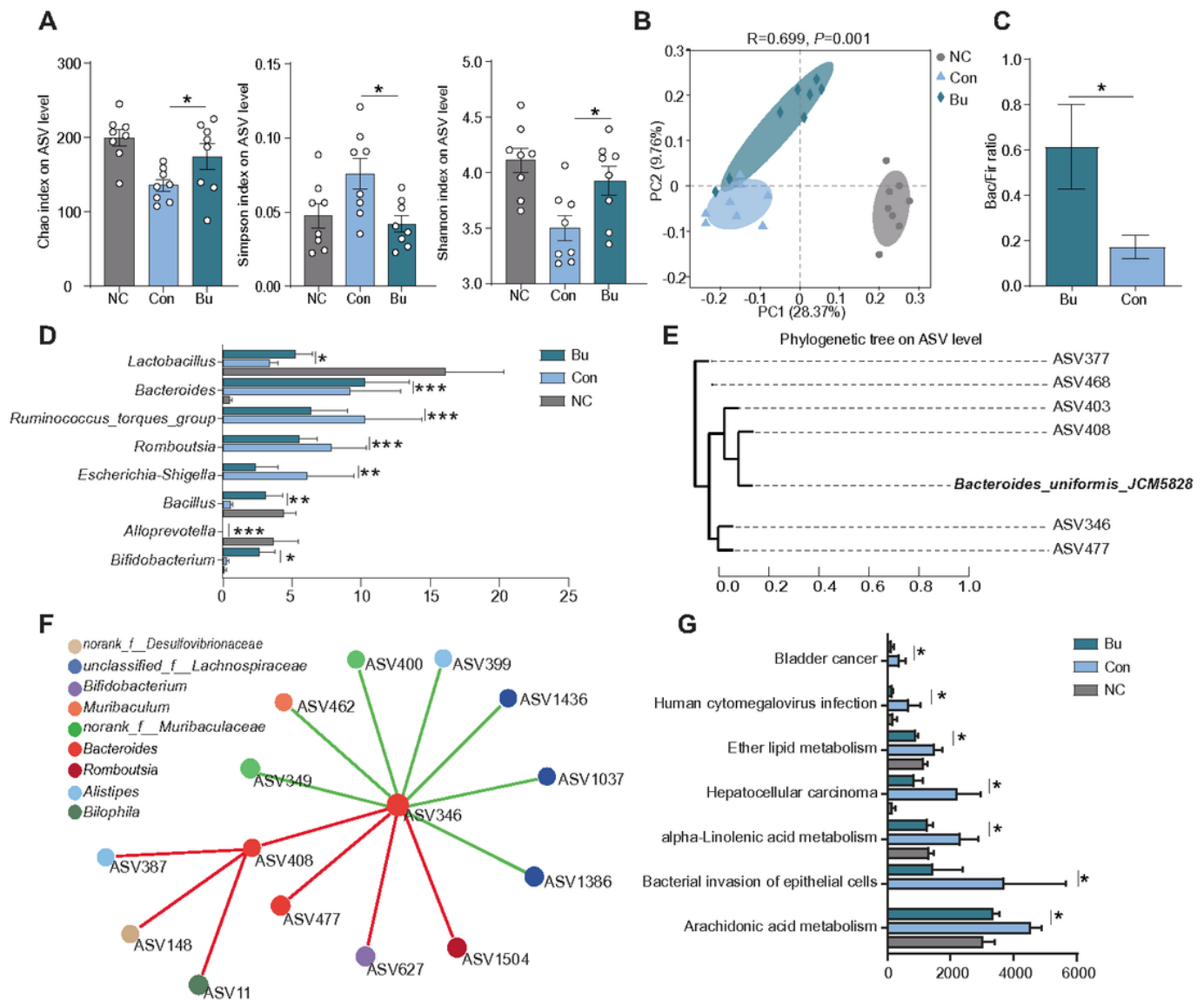
Figure 2

B. uniformis JCM5828 ameliorates DSS-induced colitis by reshaping gut microbiota and potential function. (A) The α diversity based on Chao, Simpson and Shannon indexes. (female, *n* = 8 per group). The mice were euthanized after the treatment, and colonic content samples were collected for 16S rDNA

gene sequencing. *$p < 0.05$. Data were analyzed using one-way ANOVA and expressed as means ± SEM. (B) Principle coordinate analysis (PCoA) plot based on the ASV matrix of colonic microbiota in three groups. β-diversity was determined using ANOSIM analysis. (C) The Bacteroides to Firmicutes (Bac/Fir) ratio in three groups. *$p < 0.05$. Data were analyzed using one-way ANOVA and expressed as means ± SEM. (D) Bacterial genera (relative abundance in the top 20) showing significant differences in their relative abundance between the Con and Bu group. (E) Phylogenetic distribution of the most abundant ASV. The phylogenetic tree was generated using IQ-TREE (version 1.6.8) with the maximum likelihood method. (F) Colonic microbial co-occurrence network analysis based on core ASV. Spearman's rank correlation coefficient > 0.60; *P*-value < 0.05. Different colors represent different genera in the colon. The size of nodes is proportional to the relative abundance of the ASV. The red and green lines indicate a positive and negative correlations between species, respectively. (G) The potential functional pathways of colonic content microbiota based on PICRUSt2. *$p < 0.05$. Data differences were assessed using the one-way ANOVA with Tukey's test.
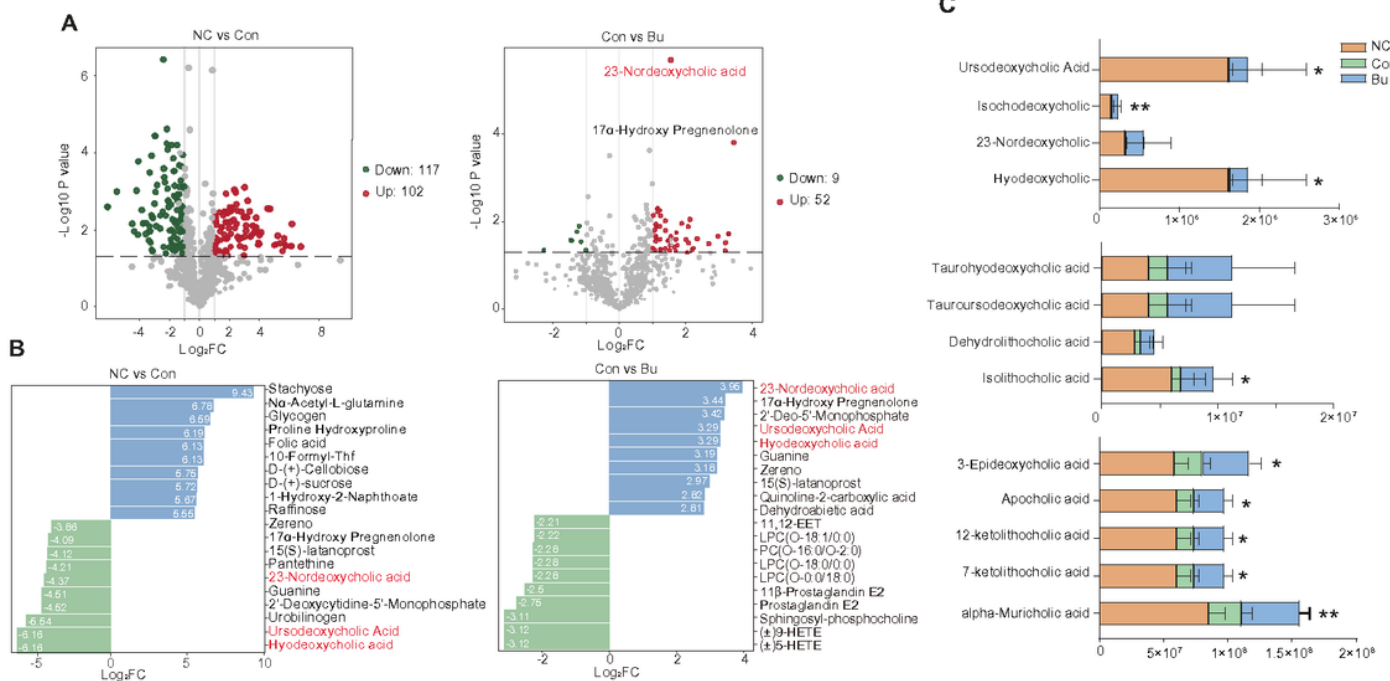

Figure 3

Figure 3

B. uniformis JCM5828 restores DSS-mediated reduction in colonic primary and secondary bile acid abundance. (A) Volcano plots for the RNA-Seq analyses of NC *vs.* Con and Con *vs.* Bu groups. The red and green circles represent up-regulated and downregulated differential metabolites, respectively. (female, *n* = 8 per group). (B) Differential metabolites bar chart in NC *vs.* Con and Con *vs.* Bu groups. The x-coordinate represents log2 value of the differential multiple, while the y-coordinate represents the

metabolite. (C) The relative abundance of 13 differential metabolites in three groups. Differential metabolites were defined as metabolites with a fold change ≥ 2 and ≤ 0.5.
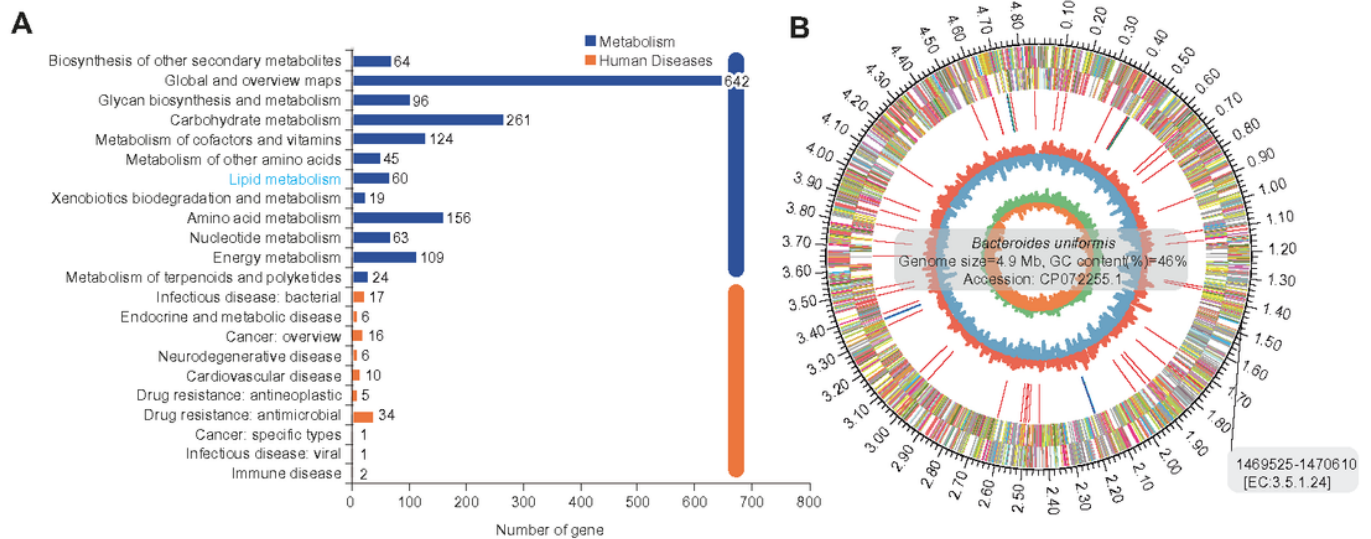
Figure 4

Figure 4

The genome of *B. uniformis* is enriched in genes related to bile acid salt conversion. (A) KEGG pathway annotated classification statistics. The vertical and horizontal coordinates indicate level 2 hierarchical classification of the KEGG pathway and the number of genes under the annotated classification, respectively. The different bar colors represent level 1 classification of the KEGG pathway. (B) Genomic circos Map of *B. uniformis*. The outermost circle, second and third circle represent the genome size, CDS on positive and negative strands, respectively. Different colors indicate the functional classification of different COGs of CDS. The fourth circle represents rRNA and tRNA. The fifth circle represents GC content. The outward red part indicates that the GC content of the region is higher than the average GC content of the whole genome, and the higher peak indicates a larger difference. The inward blue part indicates that the GC content of the region is lower than the average GC content of the whole genome, and the higher peak indicates a larger difference. The innermost circle represents the GC-Skew value.
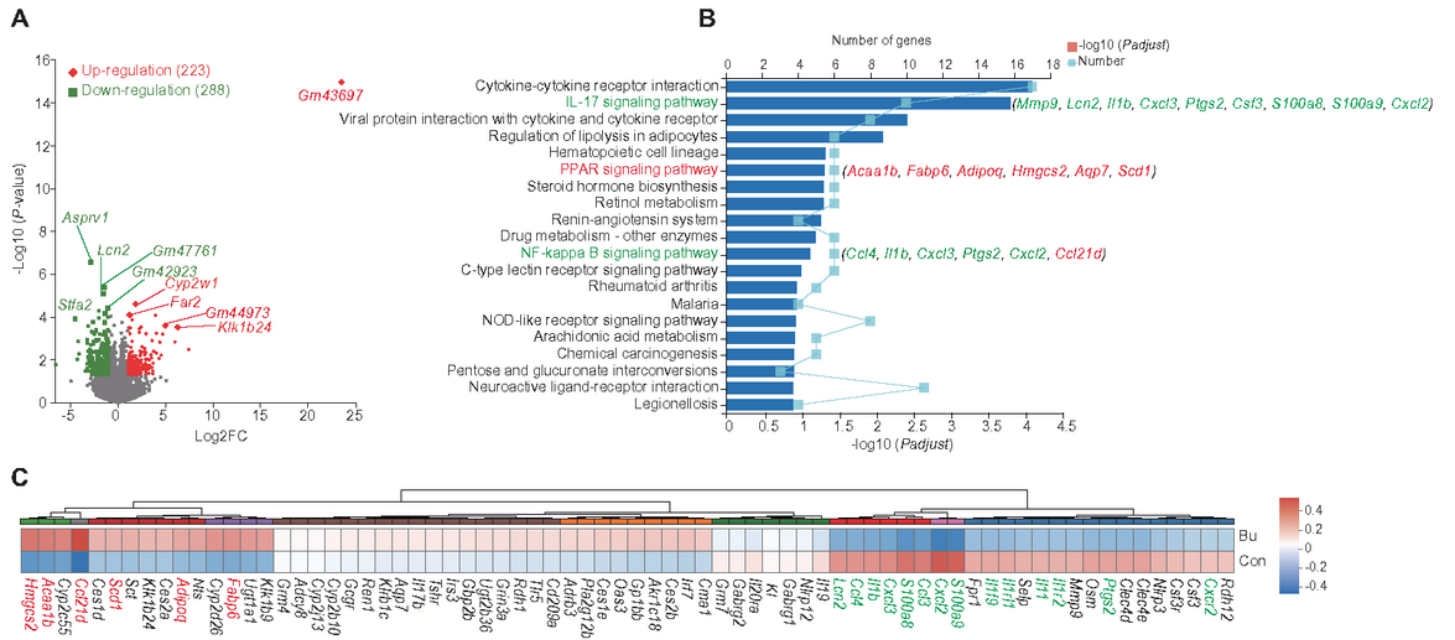
Figure 5

Figure 5

B. uniformis JCM5828 alters colonic transcriptome profile in mice with DSS-induced colitis. (A) Volcano plots for the RNA-Seq analyses of Con *vs.*Bu group. The red and green diamonds represent up-regulated and downregulated DEGs, respectively. (B) The KEGG enrichment analysis of Con *vs.* Bu group. The genes behind each bar represent the gene involved in the pathway. The red and green genes represent up-regulated and downregulated DEGs, respectively. (C) The heatmap of DEGs expression in two groups.
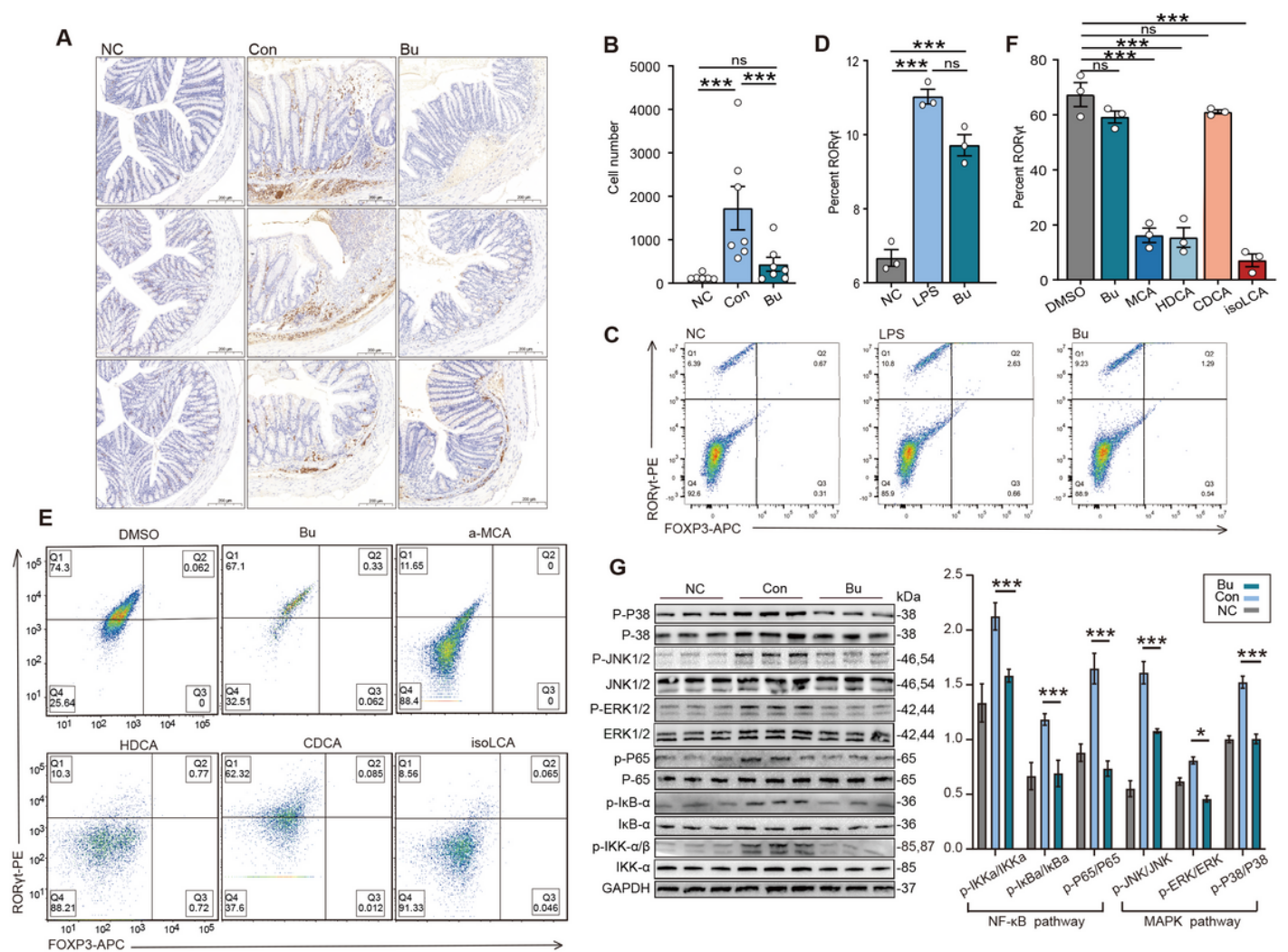
Figure 6

Figure 6

B. uniformis JCM5828-mediated αMCA inhibits TH17 differentiation and alleviates DSS-induced colitis.

(A) Immunohistochemical micrographs of TH17 in the colonic tissues (scale bar, 200 μm). (B) Cell number of Fig. 6A (n = 3) ***$p < 0.001$. Data were analyzed using one-way ANOVA and expressed as means ± SEM. (C-D) Flow cytometric analyses and quantification of native T cells intracellularly stained for RORγt. Naive T cells were isolated from C57BL/6 mice. TH17 differentiation was induced via co-culture of native T cells with *B. uniformis* supernatant (induced by lipopolysaccharide) (n = 3). Data are expressed as mean ± SEM, by unpaired t-test with two-tailed P value, ***$p < 0.001$. (E-F) Flow cytometric analyses and quantification of RORγt production from C57BL/6 mice naive T cells cultured for three days under the TH17 cell polarization condition. DMSO, *B. uniformis* supernatant or bile acids (20 μM) were added after cytokine addition (n = 3). Data are expressed asmean ± SEM, by unpaired t-test with two-tailed P value, ***$p < 0.001$. (G) Western blot analyses of p-P38/P38, p-JNK1/2/JNK1/2, p-ERK1/2/ERK1/2, p-P65/P65, p-IκB/IκB, and p-IKK/IKK in colon tissues using the respective anti-phospho-

protein antibodies, and quantified phosphorylated protein and total protein density. Data are expressed as mean ± SEM (n = 3). * $p < 0.05$, ***$p < 0.001$.
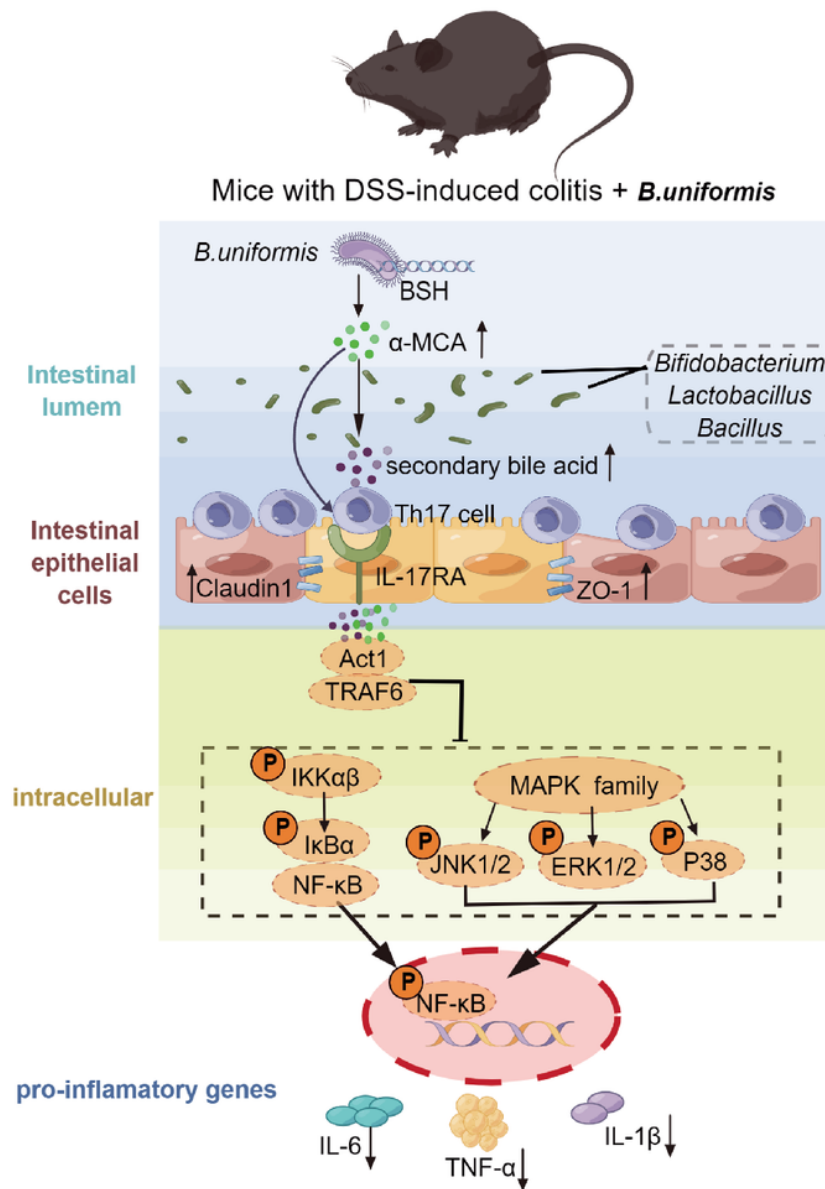
Figure 7

Figure 7

The processes behind protective effect of *B. uniformis* **JCM5828 against DSS-induced colonic inflammation in mice are summarised in a schematic picture.** *B. uniformis* gavage changed the colonic microbial composition of mice with DSS-induced colitis, and α-MCA reduced TH17 cell development and enhanced intestinal barrier function via the B. uniformis core functional enzyme gene BSH and other putative probiotic-mediated secondary bile acids. TH17 cells in the colon epithelium bind to the IL-17 receptor (IL-17R) and inhibit downstream NF-B and MAPK signaling pathways via the signaling complex

IL-17R-ACT1-TRAF6. This reduces the expression of inflammatory factors such *TNF-α*, IL-1β, and IL-6, modulating the intestinal immune response. Figdraw software was used to create this illustration.

Supplementary Files

This is a list of supplementary files associated with this preprint. Click to download.

- SupplementaryTable15.xlsx
- SupplementaryMaterials.pdf